Damage detection in compressed natural gas (CNG) cylinders based on auxiliary mass induced frequency shift

Lie Seng Tjhen[a], Zhang Yao[a*], Wang Longqi[a]

[a] School of Civil & Environmental Engineering, Nanyang Technological University,

50 Nanyang Avenue, Singapore 639798

Abstract

This paper proposes a new damage detection method for cylindrical shell structures based on the frequency shift induced by an auxiliary mass. The natural frequency of a cylindrical shell changes when an auxiliary mass is placed at different positions on its surface. In fact, when the auxiliary mass is approaching the damage resulting in a decrease of local stiffness, the natural frequencies will drop drastically. This is because the auxiliary mass increases the local mass. That is, the auxiliary mass can enhance the influence of the damage on the dynamic characteristics of the cylindrical shell, and therefore, it can be used to probe the damage by traversing it over the entire surface of the cylindrical shell. On the other hand, the sudden drop of natural frequencies induced by the auxiliary mass approaching the damage can be considered as an anomaly since the frequencies usually change smoothly under the assumption that intact cylindrical shell is homogeneous and smooth. To detect the anomaly, a new damage index is proposed based on the curvature of frequency shift, which only uses the information from the damaged cylindrical shell. The proposed method is then tested on a damaged CNG cylinder; it demonstrates that it is more accurate and sensitive compared to other traditional vibration based damage detection methods which depend on mode shape instead.

Keywords: Auxiliary mass; compressed natural gas (CNG); cylindrical shell; damage detection; frequency shift

[*] Corresponding author: Tel.: +65-67905284
Email address: yzhang30@e.ntu.edu.sg

1. Introduction

Cylindrical structures such as compressed natural gas (CNG) cylinder, pressure vessels and pipelines are usually subjected to high stresses. The initiation and propagation of damage in cylindrical shells may cause catastrophic failure. Therefore, it is important to detect damages such as corrosion and cracks at the earlier stage. To identify the structural damage, several NDT methods have been proposed and developed for the past decades; for example, visual inspection, liquid penetrant testing, magnetic particle inspection, radiographic inspection, thermal testing, ultrasonic testing, magnetic flex leakage and eddy current testing, acoustic emission testing, electromechnical impedance testing, *etc.* [1]. They have been widely applied for pressure vessels and pipeline structures in practice. In particular, eddy current testing shows good performance in metallic pipeline health integrity monitoring because it is sensitive, non-contact and does not require coupling medium [2-3]. Acoustic emission testing has been effectively used for leakage detection and stress wave monitoring, arising from local energy release induced by impacts and crack propagation [4-6]. Electromechanical impedance based NDT methods has also become popular since it is sensitive to local defects and can be used for long term real time monitoring [7-8]. Recently, Guided Ultrasonic Waves (GUWs) which overcome the drawbacks of conventional ultrasonic testing has received a lot of attention; it is especially effective for structures having one dimension much smaller than the other two, such as plates, solid cylinders and hollow cylinders [1, 9]. It is capable of probing moderately long distance and large area by few probes attached or embedded in structures while maintaining high sensitivity to small cracks and notches. Moreover, with the help of advanced sensors, it is feasible for long term structural health monitoring. The theoretical foundation of GUWs propagated in pipelines was well established [10, 11] and the capacity of GUWs to identify defects in pipes or cylindrical shells has also been demonstrated by several experimental tests [12-17]. In order to denoise the signal, extract more damage-sensitive features and improve the performance of GUWs, several advanced signal processing techniques such as wavelet analysis and empirical mode decomposition have been applied; some pattern recognition approaches have also been utilized to

inspect the structures automatically, for example, artificial neural network and support vector machine [16-18]. Usually the GUWs based methods require recorded data from a pristine structure as baseline, which is difficult in practice and limits its application. Bagheri *et al.* [18] and Lee *et al.* [19] proposed novel methods to avoid the requirement of baseline data. Moreover, Pristone *et al.* [20] extended the GUWs based NDT method to underwater structures by using noncontact laser system.

The vibration based method is also a promising alternative as it shows great advantages such as low cost and flexible measurement [21]. Except for conventional dynamic characteristics (natural frequencies, mode shapes [22-23], damping), several novel and advanced vibrational concepts (model strain energy, flexibility matrix and flexibility curvature) have been proposed to identify the location of damages and even to quantify the severity of these damages. However, most of them have been applied only to beam and plate structures and very few for cylindrical structures. Several researchers have used conventional dynamic characteristics directly to identify damages in cylindrical shells. Ip and Tse [24] proposed an approach based on frequency sensitivities and mode shapes; Sarker et al. [25] also demonstrated that the curvature of mode shapes was sensitive to local damage. Lee et al. [26-27] illustrated that multiple directional damages can be identified by using Frequency Response Functions (FRFs). Other researchers developed several promising approaches based on advanced dynamic properties. Srinivasan and Kot [28], Marwala and Hunt [29], Hu et al. [30] used the model strain energy method which was proposed for plates to detect damages in cylindrical shells. However, almost all the above mentioned methods depend highly on the quality of measured FRFs or mode shapes which are usually not accurate enough in practice. Royston et al. [31] found that the axisymmetric cylinder losing its symmetry due to local damage would cause spilt-mode phenomenon resulting in the degenerate modes to non-generate, and hence, this can be used to detect local damage in cylinders.

Low [32] analyzed the influence of multiple lump masses on the changes of beam frequencies trough Rayleigh estimation and eigen-analysis solutions. Zhong and Oyadiji [33] further analyzed the

influence of an auxiliary mass on the frequencies of a cracked beam, based on which they [34] developed a method to detect these cracks by utilizing wavelet transform. Subsequently they [35] utilized the derivative of natural frequency based on auxiliary mass spatial probing and they found that it is sensitive to local damage like cracks in beam-like structures. Zhang and Xiang [36] analyzed analytically the relationship between the natural frequency and the location of the auxiliary mass on beam-like structures, and they found that it is equivalent to the mode shape square, the curvature of which is sensitive to local damages. Later, Zhang et al. [37] extended this method to plate structures and they verified that the curvature of Frequency Shift Surface which represents the natural frequency with respect to the location of auxiliary mass is effective in local damage detection.

This study extends the concept of auxiliary mass induced frequency shift to cylindrical shape structures. It shows that when the auxiliary mass is approaching the damage where the local stiffness decreases, the natural frequencies drop drastically since the auxiliary mass increases the local mass. That is, the auxiliary mass can enhance the influence of the damage on the dynamic characteristics of the cylindrical shell, and therefore, it can be used to probe the damage by traversing it over the entire surface of the cylindrical shell. On the other hand, the sudden drop of natural frequencies caused by the auxiliary mass approaching the damage can also be considered as anomaly since the frequencies change smoothly under the assumption that intact cylindrical shell is usually homogeneous and smooth. In order to detect the anomaly, a new damage index is proposed based on the curvature of frequency shift and it uses only the information from the damaged cylindrical shell. Its accuracy and simplicity to use is demonstrated on a damaged 7-litre CNG cylinder.

2. Auxiliary mass induced frequency shift

The natural frequencies are global dynamic characteristics which usually contain limited spatial information, and therefore, they are not used directly to detect the location of damage. Instead, an auxiliary mass is utilized to make the natural frequencies contain the spatial information. In fact, when the auxiliary mass is probing the cylinder, the natural frequencies change with respect to the

location of the auxiliary mass. This can be are demonstrated by using the following model of auxiliary mass – cylinder interactive system.

As shown in Fig. 1, the auxiliary mass is simulated as spring-mass system with mass of M and stiffness of k; and it is mounted on the cylindrical shell at (θ_0, l_0) which has length of L, radius of r, thickness of h, Young's Modulus of E and density of ρ. Local damage located at (θ_d, l_d) is simulated by reducing the thickness by Δh.

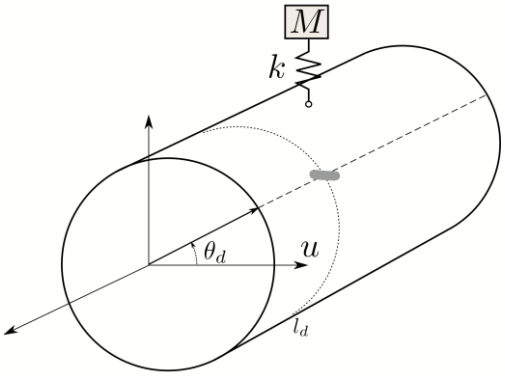

Fig. 1. The model of auxiliary mass-cylinder interactive system

If only the ring-like radial vibration is considered, the governing equations [38] can be obtained as

$$\frac{EI}{r^4}\left(\frac{\partial^4 u}{\partial\theta^4}+2\frac{\partial^2 u}{\partial\theta^2}+u\right)+\rho hL\frac{\partial^2 u}{\partial t^2}=f(t)\delta(\theta-\theta_0,l-l_0) \tag{1}$$

$$M\ddot{q}(t)+kq(t)=ku(\theta_0,l_0,t) \tag{2}$$

where $u(\theta, l, t)$ and $q(t)$ are the radial displacement of the ring and vertical displacement of the auxiliary mass respectively; δ is the Dirac delta function and $f(t)\delta(\theta-\theta_0, l-l_0)$ is the contact force:

$$f(t)=kq(t)-ku(\theta_0,l_0,t)-Mg=-M(g+\ddot{q}) \tag{3}$$

The mode shapes can be presented as

$$\varphi_{+nq}(\theta,l)=\cos\left(n\left[\theta-\theta_d\right]\right)Q_q(x) \tag{4}$$

$$\varphi_{-nq}(\theta,l)=\sin\left(n\left[\theta-\theta_d\right]\right)Q_q(x) \tag{5}$$

where n and q indicate the number of nodal points on circumferential and longitudinal directions respectively. In this respect, the signs "+" and "-" usually indicate a pair of degenerate modes having identical natural frequency value [31]. In this study, only the ring-like motion is considered so that there should be no nodal point on longitudinal direction and q should be equal to zero. It should be noted that if the cylindrical shell is extensively long, there may be several nodal points on longitudinal direction and therefore, the situation will become more complicated. In particular, if the length of the cylindrical shell is much larger than the diameter, i.e. 10 times larger, the cylindrical shell can be considered behaving as a beam with circular hollow cross section instead, and corresponding vibration based damage detection methods can be applied accordingly [38].

By using the modal superposition method, the natural frequencies of the cylinder – auxiliary mass system [38] can be obtained as

$$\omega_{\pm nq}^2(\theta_0,l_0)=\frac{\omega_{\pm c,nq}^2(\theta_0,l_0)}{1+\dfrac{M}{\rho hL\Omega_{\pm n,q}}\varphi_{\pm nq}^2(\theta_0,l_0)} \tag{6}$$

where

$$\Omega_{\pm n,q}=\int_0^L\int_0^{2\pi}\varphi_{\pm nq}^2(\theta,l)\,\mathrm{d}\theta\mathrm{d}l \tag{7}$$

and $\omega_{\pm c,nq}(\theta_0,l_0)$ are the natural frequencies of the cylindrical shell itself. Usually, they change quite slightly even though there is serious local defect and therefore they are assumed unchanged herein. More detailed derivation of Eq. (1-7) can be found in Ref. [38]. From Eq. (6), it can be found that the natural frequencies of the cylinder – auxiliary mass system will change with respect to the location of auxiliary mass, (θ_0, l_0); therefore, it can be used to probe the dynamic characteristics by traversing the entire surface of the cylinder. Especially, when it is closed to the damage, it can

amplify the effect of the damage to the dynamic characteristics of the cylinder. According to Eq. (7), heavier auxiliary mass produces larger shift of frequency. In particular, if the auxiliary mass is very small and negligible, the frequency will not change irrespective where the auxiliary mass is attached, and this coincides with condition of conventional vibration testing. In this particular case, the proposed method will fail to detect local defect. When an actual testing is carried out, the auxiliary mass should be sufficiently heavy so that the difference of frequencies at two adjacent test points is larger than the resolution of frequency; otherwise the calculation of curvature will not be accurate. Generally, the performance is better if the auxiliary mass is heavier [37-38]. However, if the auxiliary mass is too heavy, the assumption used to derive Eq. (7) that the cylindrical shell displacement can be represented as the summation of modal displacements will not be effective and this makes the situation too complicated. Therefore, the auxiliary mass having a weight more than one tenth of the overall mass of the structure is not recommended.

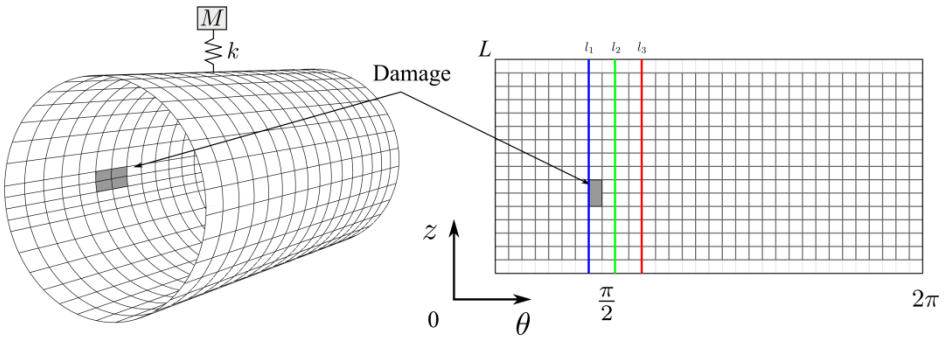

Fig. 2. Finite element model of cylinder – auxiliary mass interactive system

A simple numerical example is utilized here to illustrate the frequency shift induced by auxiliary mass. The cylindrical shell has a length $L = 330$ mm, radius $r = 160$ mm, thickness $h = 6$ mm, elastic modules $E = 2\times10^{11}$ N/m^2 and density $\rho = 7800$ kg/m^3. The auxiliary mass is 0.2 kg and the spring has stiffness of 1×10^7 N/m. An artificial damage is introduced to the cylindrical shell at $[7\pi/16, \pi/2] \times [5L/16, 7L/16]$, by reducing the thickness from 6 mm to 5 mm. The cylindrical shell is meshed into 32 parts on the circumferential direction and 14 parts on the longitudinal direction from $L/16$ to $15L/16$

(Fig. 2). Firstly, the auxiliary mass is fixed at one cross point and the frequency of the auxiliary mass - cylinder system can be calculated by ABAQUS 6.11 general purpose finite element software. Then the auxiliary mass is transferred to another cross point and the frequency can be calculated once more. Finally, the frequency surface of the damaged cylindrical shell with an auxiliary mass passing over the total 32×15 cross points can be obtained as shown in Fig. 3 [39]. Usually, the fundamental natural frequency can be measured most easily and accurately, therefore, only the fundamental natural frequency is considered in this study. For this case, n = 0, ± 1 are related to the rigid body motion, therefore, n = 2 indicates the fundamental vibration mode.

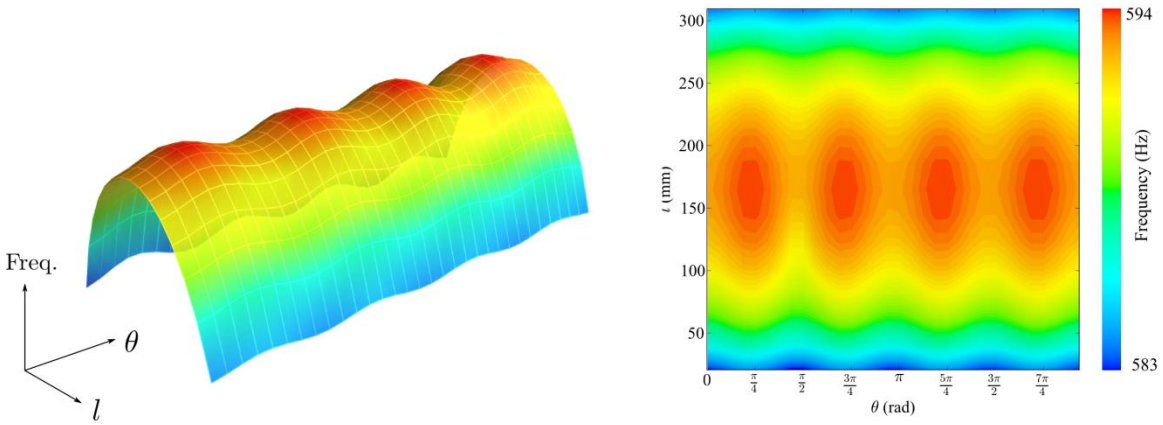

Fig. 3. The fundamental frequency surface of the damaged cylindrical shell

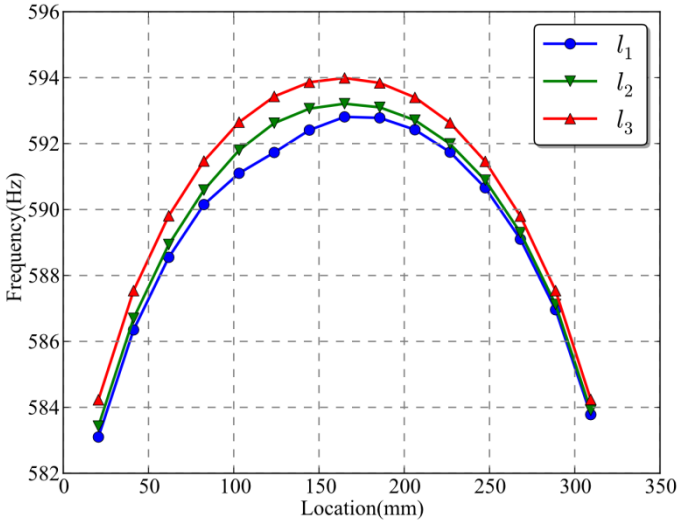

Fig. 4. The fundamental frequency curves of l_1, l_2 and l_3

As shown in Fig. 3, the fundamental frequency is never a constant but changes with respect to the location of the auxiliary mass. Moreover, the frequency surface of the damaged cylinder is quite smooth. There are four periodic fluctuations on the circumferential direction (θ) which are related to the fundamental circumferential mode shapes (n = 2) of the cylinder [31]; while on the longitudinal direction each frequency curve has a similar shape. For better illustration, three lines, l_1, l_2 and l_3 are selected which can be seen in Fig. 2. l_1 passes through the damage area but l_2 and l_3 do not. The frequency curves of l_1, l_2 and l_3 are shown in Fig. 4: they are smooth and they have quite similar shapes. It seems that it is difficult to identify the damage directly from the graphical plot; the objective of this work is to propose a simple method based on the frequency surface.

3. Damage index based on auxiliary mass induced frequency shift

The curvature is usually used to enhance the effect of anomaly [36-37], and therefore, it is also utilized in this study. The curvatures of frequency curves of l_1, l_2 and l_3 are shown in Fig. 5. It can be seen that the curvatures of frequency curves of l_2 and l_3 are quite similar and still smooth but an obvious peak appears on the curvature of frequency curve of l_1, which indicates the local damage.

That is, the curvatures of frequency curves along longitudinal direction are sensitive to the local damage, and they have very similar shapes. Since the local damage, especially at the early stage, is usually small; therefore, most curvatures of frequency curves along longitudinal direction are smooth and they almost have the same shape. Then, the average of all curvatures of frequency curves along longitudinal direction should be smooth, and it can be used as a reference to avoid the requirement of prior information from the undamaged structure. By comparing the difference between the reference and each curvature of frequency curve along longitudinal direction, the damage index can be calculated. The frequency curves along the circumferential direction usually quite smooth even if there is local defect [38]; and they fluctuate periodically and therefore, the corresponding curvatures calculated by central difference contain larger numerical errors. As a result, the curvatures of frequency curves on circumferential direction are not used here.

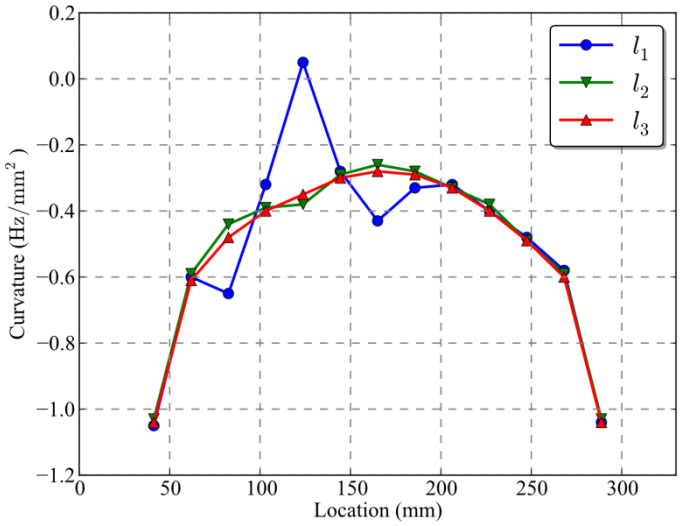

Fig. 5. The curvatures of frequency curves of l_1, l_2 and l_3

For a cylindrical shell having been meshed into uniform M×N parts on the circumferential and axial direction respectively, there should be M frequency curves along longitudinal direction and there are N+1 points on each frequency curve. In this study, $\omega(\theta, l)$ is used to represent the natural frequency, and therefore, the frequency on each cross point can be represented as $\omega(\theta_i, l_j)$, i=1,…,M,

$j=1,\ldots,N+1$. Hence, the curvature of each frequency curve along longitudinal direction can be calculated by central difference:

$$\omega''\left(\theta_i,l_j\right)=\frac{\omega\left(\theta_i,l_{j-1}\right)-2\omega\left(\theta_i,l_j\right)+\omega\left(\theta_i,l_{j+1}\right)}{\left(\Delta l\right)^2},\ j=2,\cdots,N \tag{8}$$

Then, the average of all curvatures of frequency curves can be obtained as

$$M_\omega\left(l_j\right)=\sum_{i=1}^{M}\omega''\left(\theta_i,l_j\right)/M \tag{9}$$

Finally, the damage index can be represented as

$$D\left(\theta_i,l_j\right)=\left(\omega''\left(\theta_i,l_j\right)-M_\omega\left(l_j\right)\right)^2 \tag{10}$$

The proposed damage index of this particular case is shown in Fig. 6 from which a peak indicating the local damage can be seen clearly. On the other hand, the size of the damage can also be observed from the right side of Fig. 6, which is the contour of the damage index.

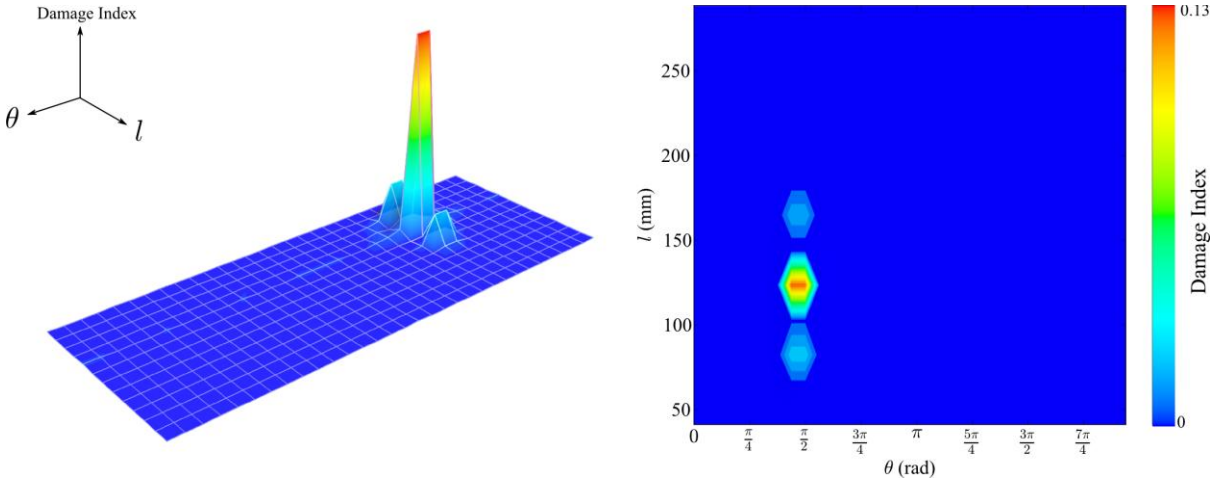

Fig. 6. Damage index of cylindrical shell with single damage

4. Damage detection of multiple damages on cylindrical shell

The numerical example of a cylindrical shell with multiple damages is adopted to validate the proposed method. The model is almost the same as that with a single damage except that another artificial damage is introduced to the cylindrical shell at $[9\pi/8,\ 19\pi/16] \times [5L/8,\ 3L/4]$ by only reducing the thickness from $6\ \mathrm{mm}$ to $5.5\ \mathrm{mm}$; and the two damages are labeled as "Damage A" and "Damage B" respectively (Fig. 7).

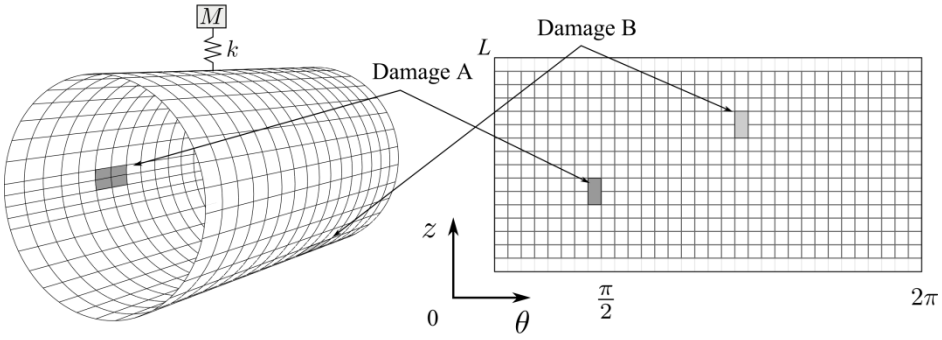

Fig. 7. The specifications of cylindrical shell with multiple damages

After the auxiliary mass is probing over the entire surface of the cylinder, the fundamental frequency surface can be obtained accordingly. The fundamental frequency surface of the cylinder with multiple damages shown in Fig. 8 is almost the same as that of cylinder with a single damage, and no obvious feature related to the damages can be found from Fig. 8. Then, the corresponding damage index can be calculated according to Eqs. (8) – (10), and the result is shown in Fig. 9. Two peaks related to "Damage A" and "Damage B" respectively can be seen clearly in Fig. 9. It also can be found from Fig. 9 that the peak indicating "Damage A" is higher than that related to "Damage B"; this is because "Damage A" is two times deeper than "Damage B", so the former is more severe than the latter. Moreover, the areas of the two peaks shown in the contour of the damage index are almost the same because the sizes of two damages are the same.

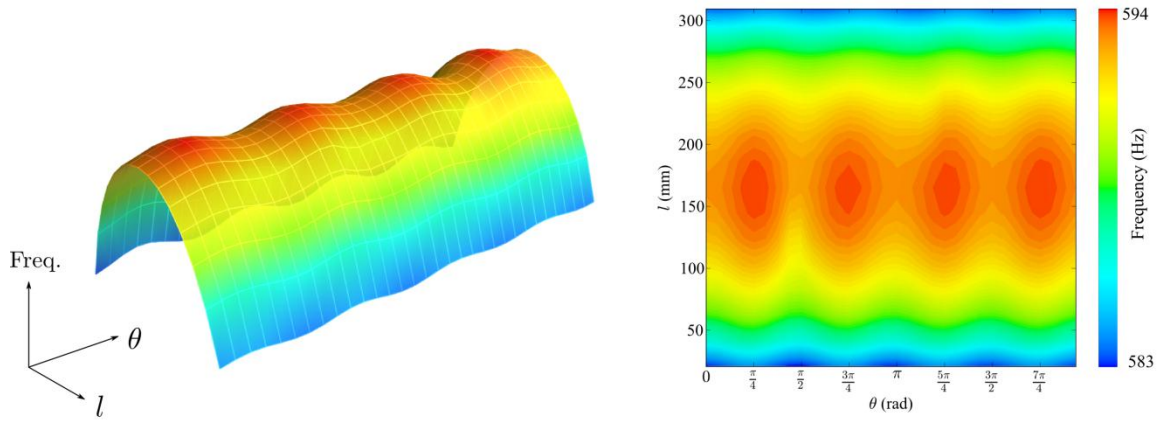

Fig. 8. The fundamental frequency surface of the cylindrical shell with multiple damages

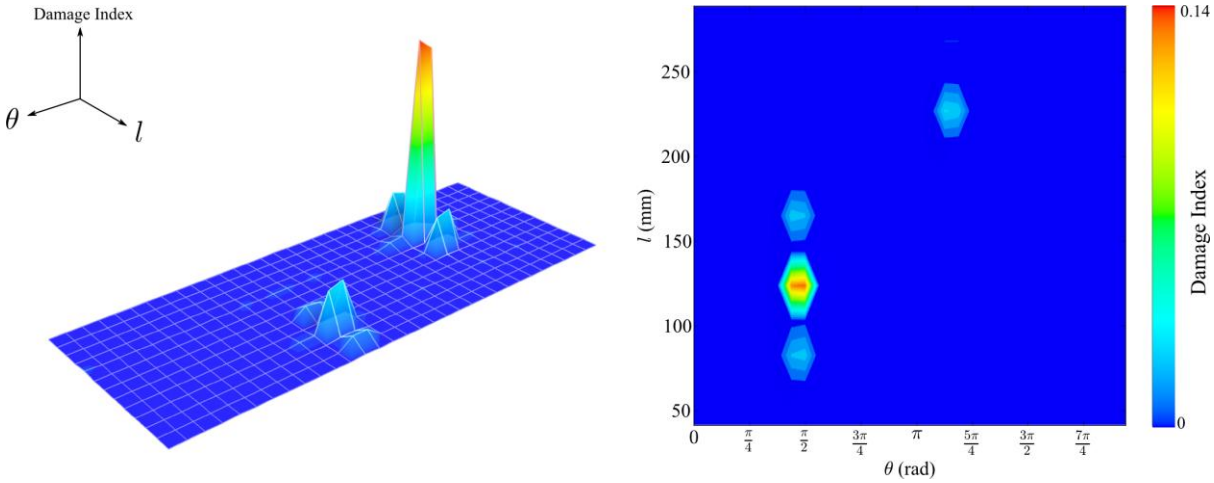

Fig. 9. Damage index of cylindrical shell with multiple damages

5. Experimental study

The proposed method is also verified by experimental testing of different damages. Firstly, a steel cylinder is utilized and an artificial local damage is introduced by reducing the thickness; after testing this single damage case, another artificial local damage is introduced to the same cylinder and this case is considered as multiple damages. Then, a 7-litre compressed natural gas (CNG) cylinder with a sharp slot simulating a crack damage is used to validate the proposed approach.

5.1. Experiment setup

The experiment setup is illustrated in Figs. 10 and 11. The specimens are supported by sponges to simulate the free-free boundary condition. For each specimen, it is meshed uniformly and the cross points are labeled clearly. A single accelerometer (Wilcoxon Model No. F3/Z602WA) is mounted at a cross point by using magnetic base and a small hammer is used to tap the specimen. The accelerometer is of 0.3 kg and it is considered as the auxiliary mass itself. As the specimen is tapped, it vibrates freely and the vibration acceleration is recorded by the accelerometer. Then, the electrical signal is amplified by a charger amplifier (Wilcoxon Model No. PA8HF) and converted to digital signal at sampling frequency of 2048 Hz by data acquisition card (Measurement Computing Model No. USB 2527). The acceleration response is analyzed by Fast Fourier Transform simultaneously (Dasylab 11) and the fundamental frequency can be obtained. The accelerometer is moved to another cross point and the fundamental frequency is recorded by using the same procedure.

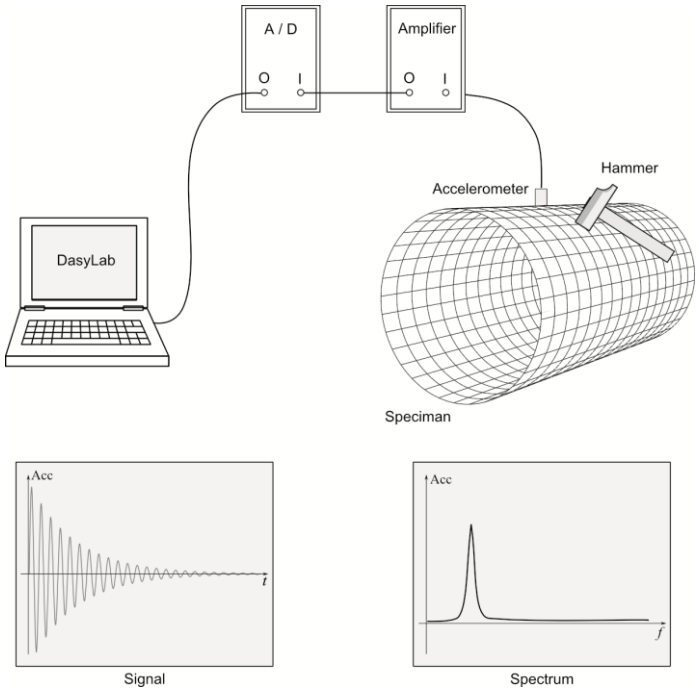

Fig. 10 The flowchart of experiment

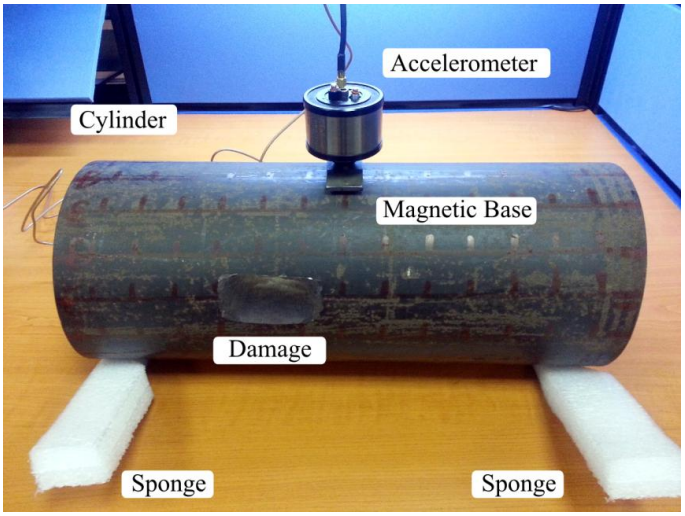

Fig. 11. The photograph of experiment setup

5.2. Steel cylinder with a single damage

A steel cylinder with a diameter D=169 mm, thickness h=6.93 mm and length L=420 mm is adopted in experiments and a single damage is introduced artificially at $[7\pi/16, 9\pi/16] \times [120\text{ mm}, 180\text{ mm}]$ by reducing the thickness by 2.5 mm as shown in Fig. 12. The cylinder is meshed uniformly into 12×16 parts and 13×16 cross points are then obtained. Therefore, there are 16 longitudinal frequency shift curves and there are 13 points on each curve.

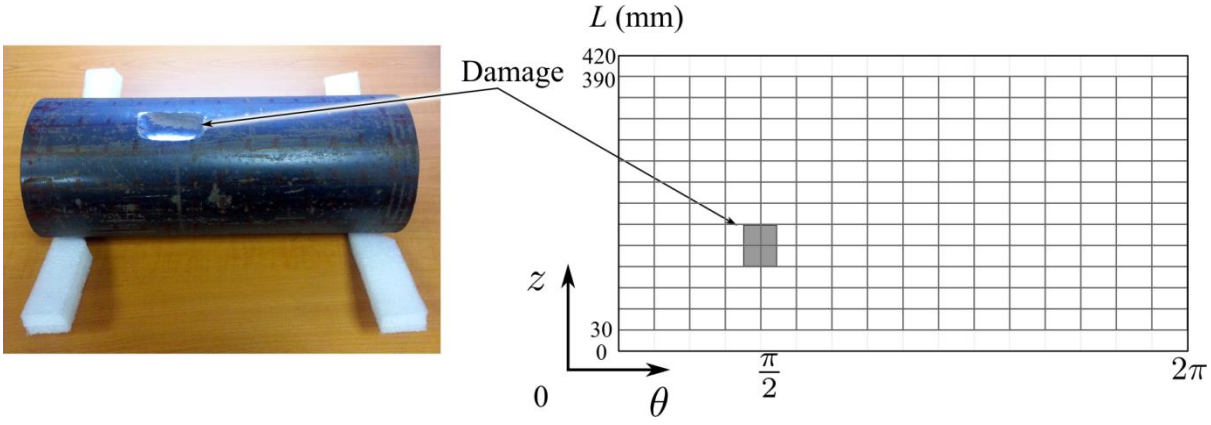

Fig. 12. The steel cylinder with a single damage

Next, the fundamental frequency surface can be obtained by following the procedures described in Section 5.1 (Fig. 10). It resembles to those in the numerical examples; however, the damage can be

indicated directly by the contour of the fundamental frequency surface. The frequency drops drastically as the auxiliary mass is approaching the local damage; this is because the local damage decreases the local stiffness while the auxiliary mass increases the local inertia. The damage index is shown in Fig. 14 from which a clear peak indicating the local damage can be seen. At the same time, the size of the damage can also be evaluated through the contour of the damage index.

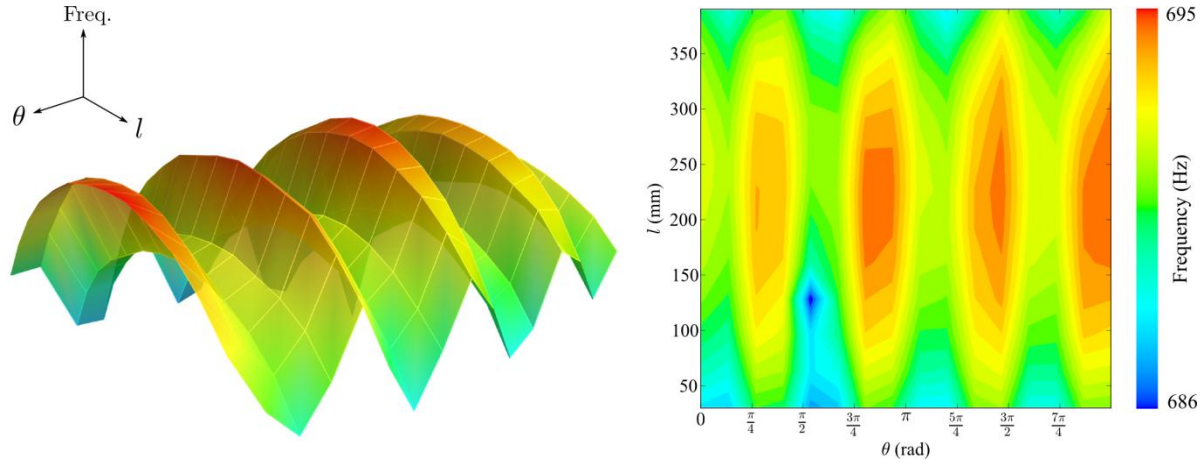

Fig. 13. The fundamental frequency surface of the steel cylinder with single damage

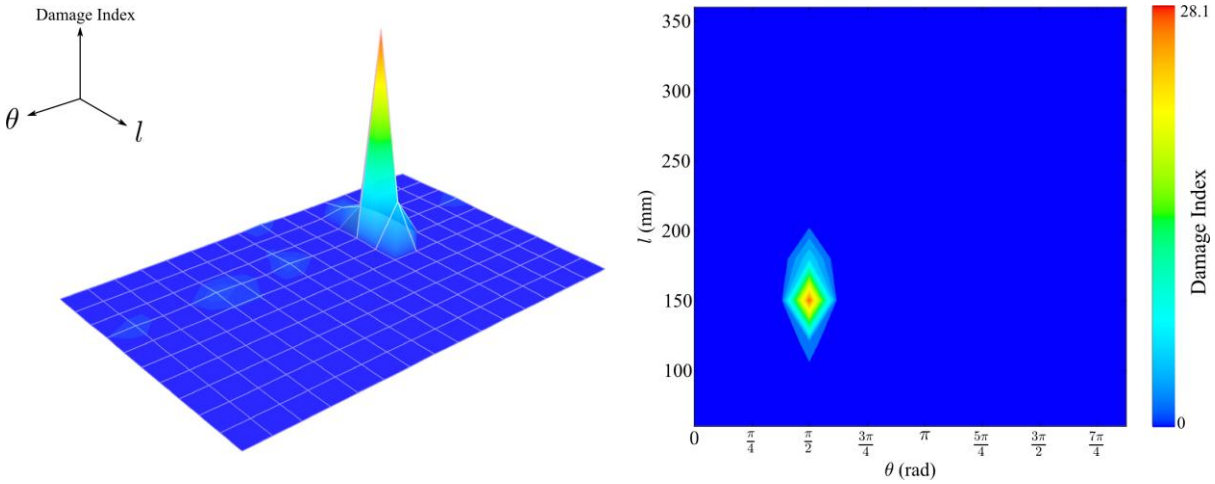

Fig. 14. Damage index of steel cylinder with a single damage

5.3. Steel cylinder with multiple damages

The same steel cylinder is used again. Another artificial damage is introduced at $[19\pi/16, 21\pi/16] \times [300\ \text{mm}, 240\ \text{mm}]$ by reducing the thickness by 0.5 mm which is labeled as “Damage B” in Fig. 15

while the previous local damage is labeled as “Damage A”. The sizes of these two damages are almost identical; however, “Damage A” is much more severe than “Damage B” because the former is five times deeper as the latter.

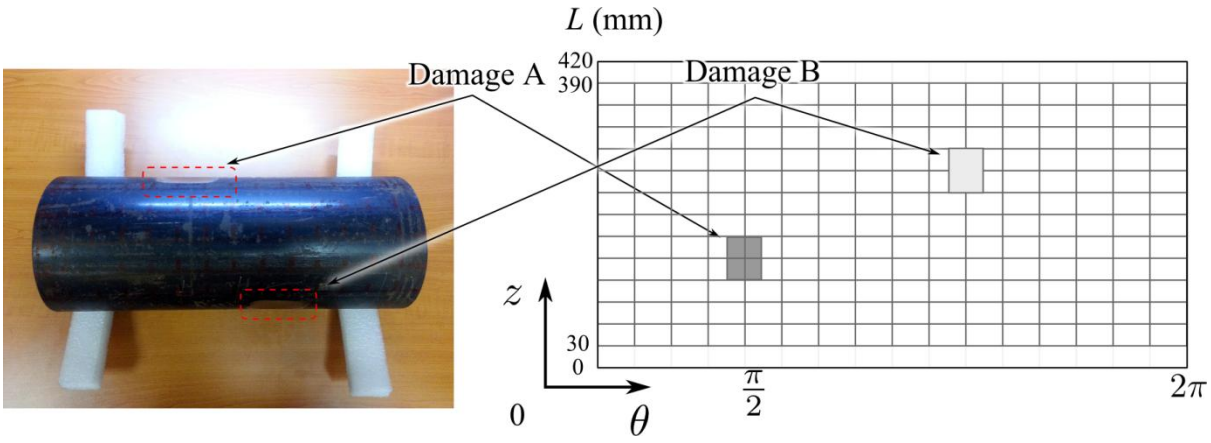

Fig. 15. The steel cylinder with multiple damages

The fundamental frequency surface and the corresponding damage index can be seen in Figs. 16 and 17 respectively. The fundamental frequency surface is quite similar to that with only a single damage; “Damage A” can be indicated clearly as a sudden drop while “Damage B” is not so obvious; this is because the former is much more severe than the latter. The same conclusion can be obtained from Fig. 17 where the peak indicating “Damage A” is much higher than that related to “Damage B”, which also validates that the damage index can describe the severity of local damages as well. Moreover, from the contour of the damage index shown at the right side of Fig. 17, the sizes of these two damages can be determined; they have similar area which coincides with those shown in Fig. 15.

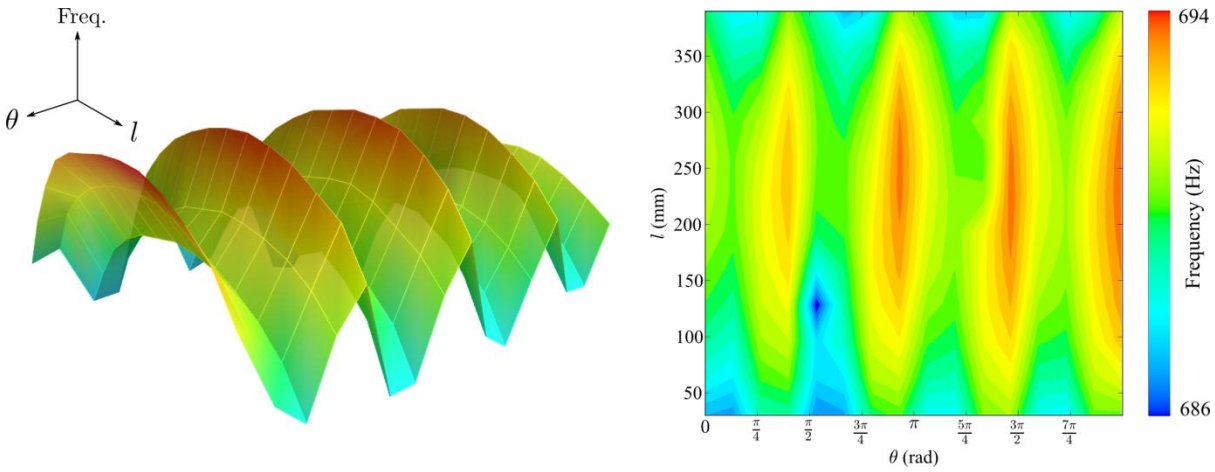

Fig. 16. The fundamental frequency surface of the steel cylinder with multiple damages

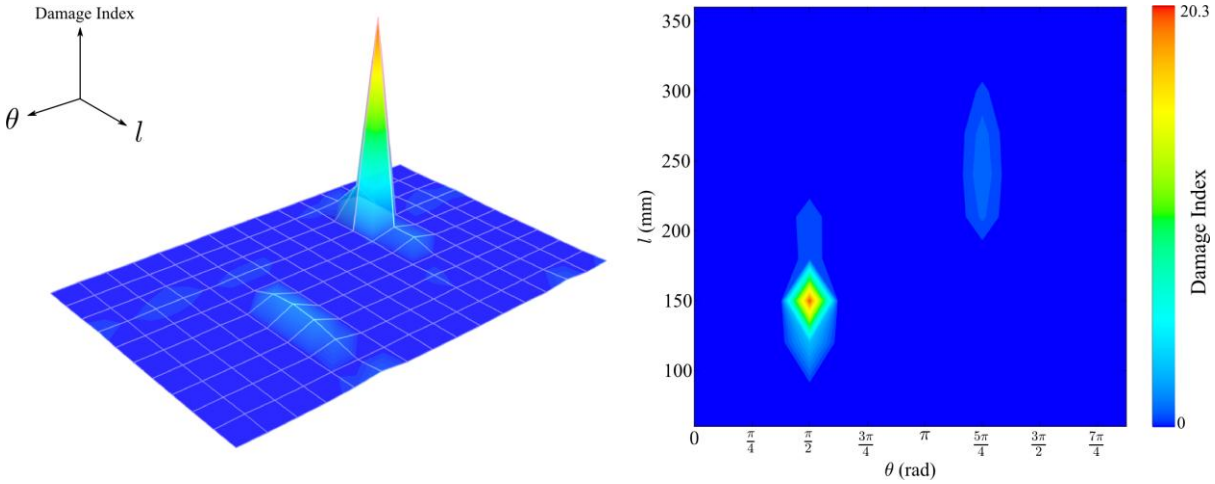

Fig. 17. Damage index of steel cylinder with multiple damages

5.4. Compressed natural gas (CNG) cylinder with artificial crack

Finally, a 7-litre CNG cylinder shown in Fig. 18 is utilized in the experiment because its main body consists of a cylindrical shell. The dimensions of the cylindrical shell part are as follows: external diameter D=170 mm, thickness h=6 mm and length L=320 mm. The cylindrical shell part is meshed uniformly into 10×16 parts and 11×16 cross points are then obtained. Then, there are 16 longitudinal frequency shift curves and there are 11 points on each curve.

A narrow slot having a width of 1mm and a depth of 5 mm is artificially cut into the CNG cylinder using an EDM machine to simulate a crack damage (Fig. 18). Without loss of generality, the slot is

located at $(7\pi/8+\pi/40) \times [80\ \text{mm}, 240\ \text{mm}]$ and no cross point is located on the slot. For this CNG cylinder, its vibration mode is different from the steel cylinder used in the previous two experiments: the steel cylinder has free-free boundary condition but the cylindrical shell part of the CNG cylinder should be considered as a fixed end boundary condition. This is because the two ends of the cylinder are much thicker than the cylinder wall and the two ends are almost stationary when the part of cylindrical shell vibrates.

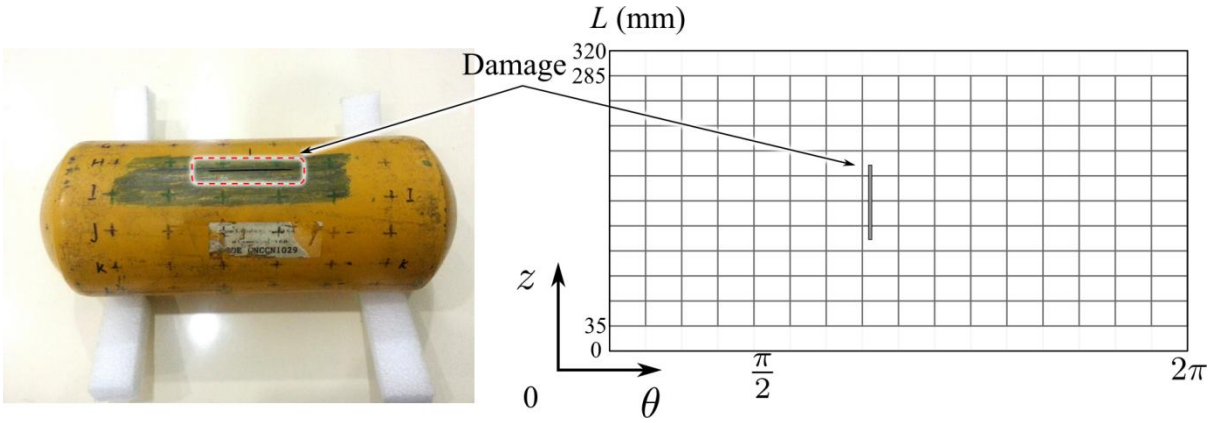

Fig. 18. The CNG cylinder containing a crack damage

The fundamental frequency surface can be measured as shown in Fig. 19. Because the boundary condition is different, the frequency surface in this case is different from the previous two cylinders as well: the frequency is lower at the middle and higher at the boundary, which is opposite to the previous two cases with free-free boundary condition. In fact, the local stiffness at the boundary area is higher due to the fixed end boundary condition, while the local stiffness at the middle area is much lower. On the other hand, the influence of the crack on the frequency surface is so large that the crack can be detected immediately from the frequency surface; the frequency near the crack drops drastically which can be seen in Fig. 19 clearly. From the damage index shown in Fig. 20, the simulated crack can be detected easily and its size can be determined as well.

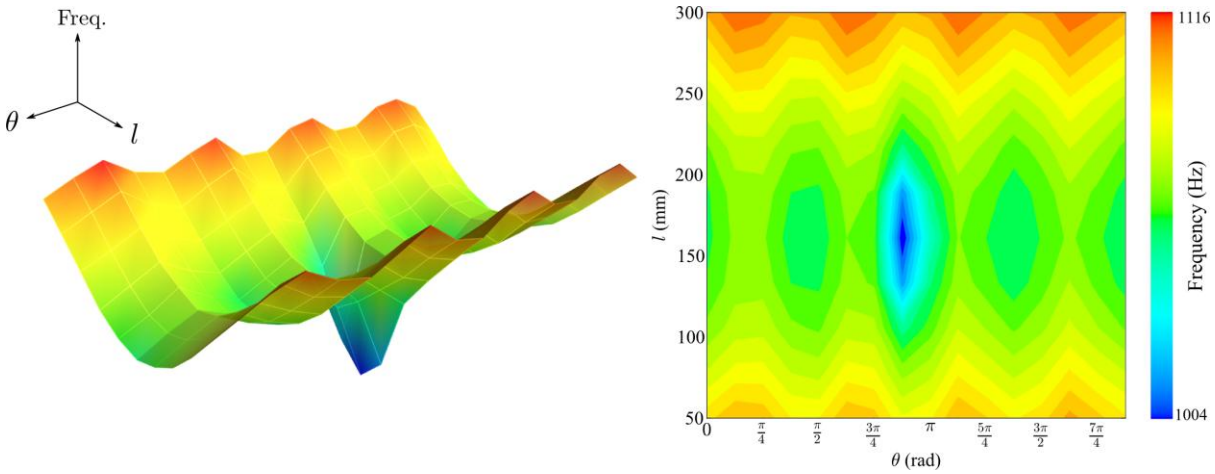

Fig. 19. The fundamental frequency surface of the CNG cylinder containing a crack damage

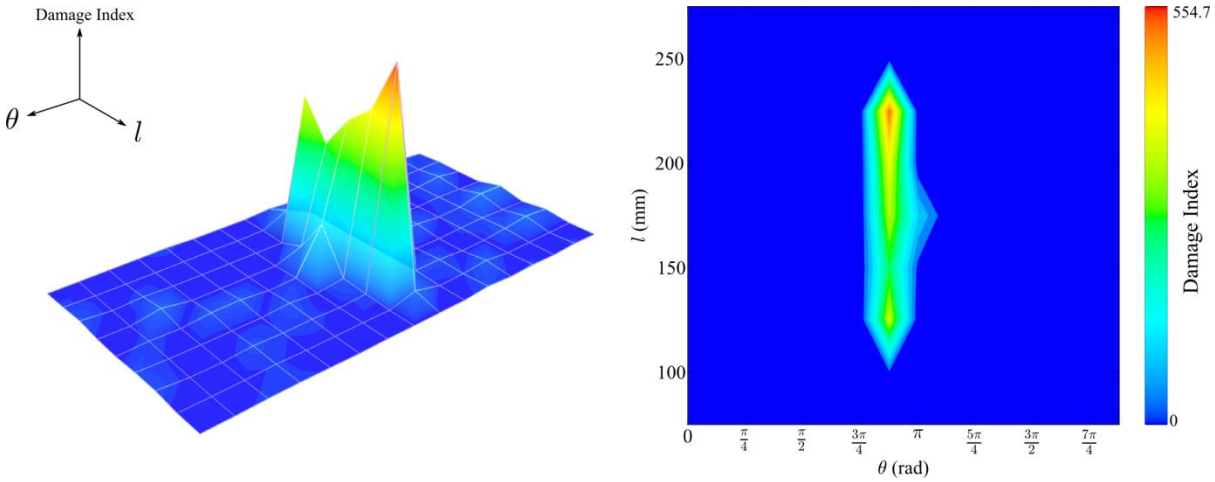

Fig. 20. Damage index of the CNG cylinder containing a crack damage

6. Conclusions and discussion

This paper develops a frequency shift based damage detection method by using auxiliary mass for cylindrical shells. It is found that the natural frequency changes with respect to the location of the auxiliary mass. When the auxiliary mass is approaching the local damage, the natural frequency drops significantly; this is because the auxiliary mass increases the local inertia while the local damage decreases the local stiffness. Therefore, the auxiliary mass amplifies the effect of local damage on the dynamic characteristics, and it can be used to probe the local damage. The selection

of auxiliary mass is important: it should be heavy enough that the difference between frequencies at two adjacent test points is larger than the resolution of frequency, and it should not be too heavy making the assumption of modal decomposition method ineffective. In order to avoid the requirement of prior information from the undamaged structure, a new damage index is proposed based on the assumption that the frequency surface of undamaged cylindrical shell is usually smooth while the sudden drop of natural frequencies induced by the auxiliary mass approaching the damage is regarded as anomaly. The damage index shows good performance which is validated by both numerical examples and experimental results. The proposed method is easy to implement in practice to inspect damaged CNG cylinders fitted in vehicles. This is because only one single accelerometer is required and no eigenvalue problem or singular value problem needs to be solved; it is also more accurate because the natural frequency can be measured more accurately than mode shapes used in conventional vibration based damage detection methods.

Although this approach is effective for part of cylindrical shell in pressure vessels, however, it cannot be directly extended to pipelines with extensive length, and further investigation needs to be carried out. As it is based on the ring-like vibrational mode where no nodal point on the longitudinal direction exists; the situation becomes more complicated once the cylindrical shell is too long like a pipeline, because there may be several nodal points on longitudinal direction. In fact, if the length of cylindrical shell is much larger than the diameter, the frequency shift on longitudinal direction is much larger than that on circumferential direction, and the extensive long cylindrical shell can be considered behaving as a beam with circular hollow cross section, and corresponding vibration based defect detection methods for beam like structures can be applied. On the other hand, the GUWs based SHM methods are particularly more effective for pipelines with extensive length, and therefore, they are more suitable for those cases.

Acknowledgements

The authors would like to thank Maritime Research Center at Nanyang Technological University, and Maritime Port Authority of Singapore for funding this project under the Project Grant No. MPA 23/04.15.03 – RDP 014/07/049.

References

[1] P. Rizzo, Water and wastewater pipe nondestructive evaluation and health monitoring: a review, *Advances in Civil Engineering* 2010 (2010) 1-13.

[2] J.B. Nestleroth, R. J. Davis, Application of eddy currents induced by permanent magnets for pipeline inspection, *NDT & E International* 40 (1) (2007) 77-84.

[3]C.S. Angani, D.G. Park, C.G. Kim, P. Leela, M. Kishore, Y.M. Cheong, Pulsed eddy current differential probe to detect the defects in a stainless steel pile, *Journal of Applied Physics* 109 (7) (2011) 07D348.

[4] D. Ozevin, J. Harding, Novel leak localization in pressurized pipeline networks using acoustic emission and geometric connectivity, *International Journal of Pressure Vessels and Piping* 92 (2012) 63-69.

[5] A. Mostafapour, S. Davoodi, Analysis of leakage in high pressure pipe using acoustic emission method, *Applied Acoustics* 74 (3) (2013) 335-342.

[6] G. Giunta, S. Budano, A. Lucci, L. Prandi, Pipeline health integrity monitoring based on acoustic emission technique, *ASME 2012 Pressure Vessels and Piping Conference* 5 277-283.

[7] Y.W. Yang and Y.H. Hu, Electromechanical impedance modelling of PZT transducers for health monitoring of cylindrical shell structures, *Smart Materials and Structures* 17(1) (2008) 015005.

[8] H. Lee, H. Sohn, S. Yang, J. Yang, Monitoring of pipelines in nuclear power plants by measuring laser based mechanical impedance, *Smart Materials and Structures* 23 (6) (2014) 065008.

[9] P. Rizzo, F. Lanza di Scalea, Wavelet-based unsupervised and supervised learning algorithms for ultrasonic structural monitoring of waveguides, Prog*ress in smart materials and structures research, Ch. 8*, Nova Editorial (2006) 227-290.

[10] D.E. Bray and R.K. Stanley, *Nondestructive evaluation. A tool in design, manufacturing and service*, (1997), CRC Press, Boca Raton, Fla, USA.

[11] D.N. Alleyne, B. Pavlakovic, M.J.S. Lowe and P. Cawley, Rapid long-range inspection of chemical plant pipework using guided waves, *Insight* 43 (2) (2001) 93-96.

[12] W.B. Na, T. Kundu, Underwater pipeline inspection using guided waves, *Journal of Pressure Vessel Technology ASME* 124 (2) (2002) 196-200.

[13] C. Lee and S. Park, Damage classification of pipelines under water flow operation using multi-mode actuated sensing technology, *Smart Materials and Structures* 20 (11) (2011) 115002.

[14] Y.J. Ying, J.H. Garrett Jr. J. Harley, I.J. Oppenheim, J. Shi, L. Soibelman, Damage detection in pipes under changing environmental conditions using embedded piezoelectric transducers and pattern recognition techniques, *Journal of Pipeline Systems Engineering and Practice* 4 (1) (2012) 17-23.

[15] P.W. Tse, X.J. Wang, Characterization of pipeline defect in guided-waves based inspection through matching pursuit with the optimized dictionary, *NDT & E International* 54 (2013) 171-182.

[16] S.A. Atashipour, H.R. Mirdamadi, M.H. Hemasian-Etefagh, R. Amirfattahi, S. Ziaei-Rad, An effective damage identification approach in thick steel beams based on guided ultrasonic waves for structural health monitoring applications, *Journal of Intelligent Material Systems and Structures* 24 (5) (2012) 584-597.

[17] H.Z. HosseinAbadi, R. Amirfattahi, B. Nazari, H.R. Mirdamadi, S.A. Atashipour, GUW-based structural damage detection using WPT statistical features and multiclass SVM, *Applied Acoustics* 86 (2014) 59-70.

[18] A. Bagheri, K.Y. Li, P. Rizzo, Reference-free damage detection by means of wavelet transform and empirical mode decomposition applied to Lamb waves, *Journal of Intelligent Material Systems and Structures* 24 (2) (2012) 194-208.

[19] H. Lee, J. Yang, H. Sohn, Baseline-free pipeline monitoring using optical fibre guided laser ultrasonics, *Structural Health Monitoring* 11 (6) (2012) 684-695.

[20] E. Pistone, K.Y. Li, P. Rizzo, Noncontact monitoring of immersed plates by means of laser-induced ultrasounds, Structural Health Monitoring 12 (5-6) 549-565.

[21] W. Fan, P.Z. Qiao, Vibration based damage identification methods: a review and comparative study, *Structural Health Monitoring* 10(2011) 83–111.

[22] A.K. Pandey, M. Biswas, M.M. Samman, Damage detection from changes in curvature mode shapes, *Journal of Sound and Vibration* 145(2) (1991) 321-332.

[23] D. Montalvao, A.M.R. Ribeiro, J.A.B. Duarte-Silva, Experimental assessment of a modal based multi-parameter method for locating damage in composite laminates, *Experimental Mechanics* 51 (9) (2011) 1473-1488.

[24] K.H. Ip, P.C. Tse, Locating damage in circular cylindrical composite shells based on frequency sensitivities and mode shapes, *European Journal of Mechanics A/Solids* 21 (2002) 615-628.

[25] L. Sarker, Y. Xiang, B. Uy and X. Zhu, Damage detection of circular cylindrical shells by Ritz method, *Journal of Physics: Conference Series* 35 (2011).

[26] U. Lee, W. Jeong, J. Cho, A frequency response function-based damage identification method for cylindrical shell structures, *KSME International Journal* 18 (12) (2004) 2114-2124.

[27] U. Lee, S. Kim, Identification of multiple directional damages in a thin cylindrical shell, *International Journal of Solids and Structures* 43 (2006) 2723-2743.

[28] M.G. Srinivasan, C.A. Kot, Damage index algorithm for a circular cylindrical shell, *Journal of Sound and Vibration* 215 (3) (1998) 587-591.

[29] T. Marwala, H. Hunt, Is damage identification using vibration data in a population of cylinders feasible, *Journal of Sound and Vibration* 237(4) (2000) 727-732.

[30] H. Hu, C. Wu, W. Lu, Damage detection of circular hollow cylinder using modal strain energy and scanning damage index methods, *Computers and Structures* 89 (2011) 149-160.

[31] T.J. Royston, T. Spohnholtz, W.A. Ellingson, Use of non-degeneracy in nominally axisymmetric structures for fault detection with application to cylindrical geometries, *Journal of Sound and Vibration* 230(4) (2000): 791-808.

[32] K.H. Low, Frequencies of beams carrying multiple masses: Rayleigh estimation versus eigenanalysis solutions, *Journal of Sound and Vibration* 268 (2003) 843-853.

[33] S.C. Zhong, S.O. Oyadiji, Analytical predictions of natural frequencies of cracked simply supported beams with a stationary roving mass, *Journal of Sound and Vibration* 311 (2008) 328-352.

[34] S.C. Zhong, S.O. Oyadiji, Identification of cracks in beams with auxiliary mass spatial probing by stationary wavelet transform, *Journal of Vibration and Acoustics* 130 (4) (2008) 1-14.

[35] S. Zhong, S. Olutunde, K. Ding, Response-only method for damage detection of beam-like structures using high accuracy frequencies with auxiliary mass spatial probing, *Journal of Sound and Vibration* 311 (3-5) (2008) 1075-1099.

[36] Y. Zhang, Z.H. Xiang, Frequency shift curve based damage detection method for beam structures, *Computers, Materials & Continua* 26 (1)(2011)19–35.

[37] Y. Zhang, L.Q. Wang, S.T. Lie, Z.H. Xiang, Damage detection in plates structures based on frequency shift surface curvature, *Journal of Sound and Vibration* 332 (25) (2013) 6665-6684.

[38] Y. Zhang, S.T. Lie, Z.H. Xiang, Q.H. Lu, A frequency shift curve based damage detection method for cylindrical shell structures, *Journal of Sound and Vibration* 333 (6) (2014) 1671-1683.

[39] P. Ramachandran, G. Varoquaux, Mayavi: 3D Visualization of Scientific Data, *IEEE Computing in Science & Engineering*, 13 (2)(2011)40-51.